



# Self-energy self-consistent density functional theory plus dynamical mean field theory

Sumanta Bhandary <sup>1,2,\*</sup> and Karsten Held <sup>1</sup><sup>1</sup>*Institute of Solid State Physics, TU Wien, 1040 Wien, Austria*<sup>2</sup>*School of Physics and CRANN Institute, Trinity College Dublin, The University of Dublin, Dublin 2, Ireland*

(Received 15 May 2020; revised 18 September 2020; accepted 26 May 2021; published 11 June 2021)

We propose a hybrid approach which employs the dynamical mean field theory (DMFT) self-energy for the correlated, typically rather localized orbitals and a conventional density functional theory (DFT) exchange-correlation potential for the less correlated, less localized orbitals. We implement this self-energy (plus charge density) self-consistent DFT+DMFT scheme in a basis of maximally localized Wannier orbitals using WIEN2K, WIEN2WANNIER, and the DMFT impurity solver W2DYNAMICS. As a test-bed material we apply the method to SrVO<sub>3</sub> and report a significant improvement as compared to previous  $d+p$  calculations. In particular, the position of the oxygen  $p$  bands is reproduced correctly, which has been a persistent hassle in DFT+DMFT before, and has unwelcomed consequences for the  $d-p$  hybridization as well as for the correlation strength. Taking the (linearized) DMFT self-energy also in the Kohn-Sham equation bypasses the uncertainty of the “double-counting” problem of DFT+DMFT and yields very similar quasiparticle renormalized bands on the “DFT” and “DMFT” side.

DOI: [10.1103/PhysRevB.103.245116](https://doi.org/10.1103/PhysRevB.103.245116)

## I. INTRODUCTION

Density functional theory (DFT) [1,2] is by far the most widely used method in solid state physics, owing to its immense success in predicting solid state properties such as crystal structures, ionization energies, electrical, magnetic, and vibrational properties. However, treating electron correlations within an effectively single-particle framework makes it inadequate, even with the best available exchange correlation potentials, for an important class of materials: strongly correlated electron systems. This is the realm of dynamical mean field theory (DMFT) [3–5] which incorporates local, dynamic correlations, and has been merged with DFT for the calculation of realistic correlated materials [6–10]. In DMFT, the electrons can stay at a lattice site or dynamically hop between lattice sites in order to suppress double occupation and hence the cost of the Coulomb interaction, without any symmetry breaking unlike in the static DFT+ $U$  approach [11]. The method has been successfully applied to transition metals [7] and their oxides [12], molecules [13,14], adatoms [15], and  $f$ -electron systems [16,17], thus proving its versatility.

The early developments in this direction are “one-shot” DFT+DMFT [18–25] calculations. In a “one-shot” calculation, first a DFT calculation is converged for a given material. Subsequently, the DFT Hamiltonian is supplemented with a local Coulomb interaction for the correlated orbitals and this problem is solved within the DMFT framework. The physical properties such as the spectral function, susceptibility, or magnetization are calculated from this “one-shot” DMFT solution of a DFT derived Hamiltonian.

Subsequently, the charge self-consistent (CSC) DFT+DMFT method has been implemented and applied. Here, the total electronic charge density is updated after the DMFT calculation, now including effects of electronic correlations. With this updated charge density, the Kohn-Sham equation of DFT is solved, a new Hamiltonian is derived which is solved by DMFT, etc. Both cycles, DFT and DMFT, are converged simultaneously. The physical properties are calculated from the converged solution. The correlation-induced change in the charge density can be significant. Hence, for some materials using CSC leads to a major correction; for other materials the corrections are minute. Incorporation of this CSC correction in a site-to-site charge transfer has been studied extensively [18–24]. More recently, also the effect of the interorbital and momentum-dependent charge redistribution has been studied [25].

While DFT provides a reasonable starting point for both “one-shot” and CSC DFT+DMFT, the incompatibility of the DFT and DMFT approach is seen in many occasions, e.g., in so-called “ $d+p$ ” DMFT calculation for transition metal oxides [24,26–31]. The reason behind this is that in DFT the  $p$  bands are too close to the Fermi level. Hence, there is a too strong intermixture of  $d$  and  $p$  bands and the  $d$  orbitals are not strongly correlated. Within the framework of DFT+DMFT, one consequently needs to introduce an adjustment to the  $d-p$  splitting, adjusting it either to the experimental oxygen  $p$  position [31,32], adding a  $d-p$  interaction parameter [26], or modifying the double-counting [24,29] or exchange-correlation potentials [33,34]. For example, in SrVO<sub>3</sub>, the proper renormalization of the  $t_{2g}$  band has been obtained with an additional shift applied to the O  $p$  bands which is as large as 5 eV relative to the  $t_{2g}$  bands [32], for correcting the position of the O  $p$  bands to that observed in experiment.

\*sumanta.bhandary@tcd.ie

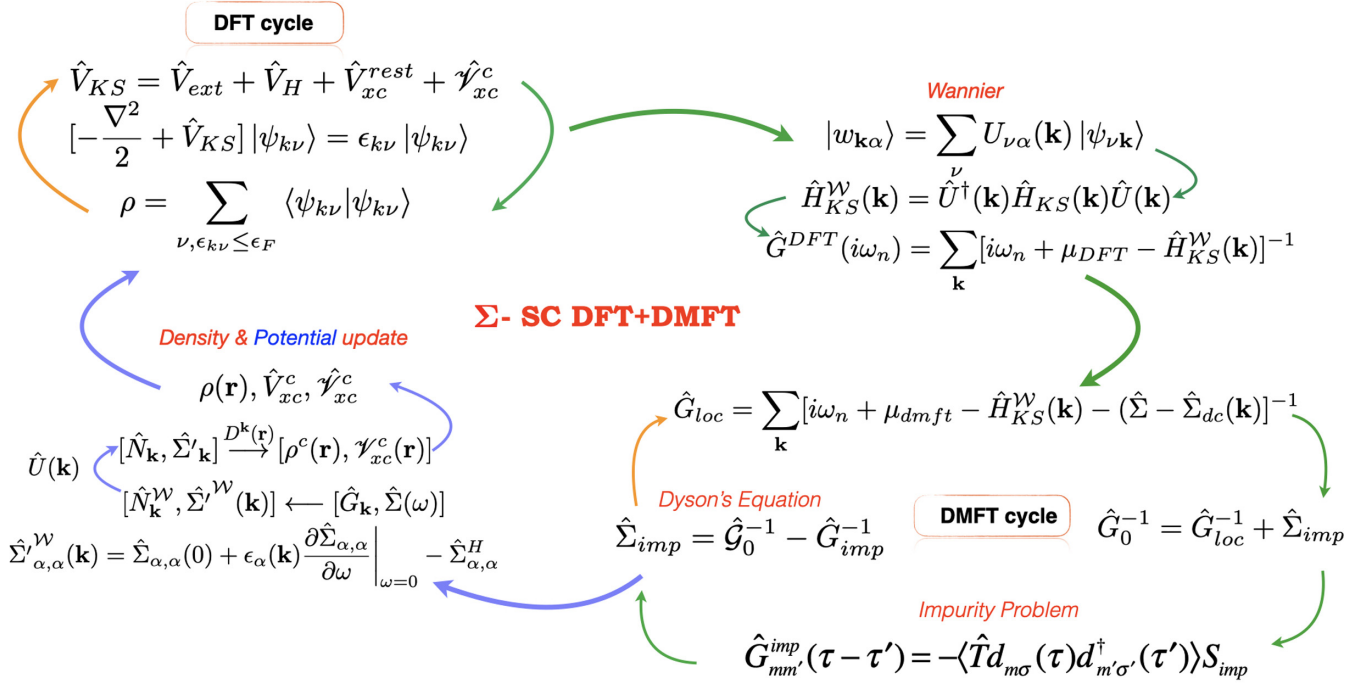


FIG. 1. Schematic representation of the  $\Sigma$ -SC DFT+DMFT. In a one-shot DFT+DMFT calculation, the DFT Hamiltonian is not updated and both the DFT and DMFT cycles close individually, i.e., we have the orange and green arrows in the schematic. In a  $\Sigma$ -SC DFT+DMFT calculation, neither DFT nor DMFT is iterated individually. Instead, both steps are closed together, i.e., we have the green and the purple arrows in the schematic, but not the orange ones.

There have been considerable efforts to improve on the exchange part of the exchange-correlation potential. Approaches in this direction include GW [35]+ DMFT [36–39] and quasiparticle self-consistent GW (QS GW) [40,41] + DMFT [42,43]; also hybrid functionals [44] instead of the more widespread local density approximation (LDA) or generalized gradient approximation (GGA) exchange-correlation potential can be employed. But, all of these approaches do not solve the problem of the wrong position of the oxygen  $p$  bands. In this paper, we propose an alternative self-energy self-consistent ( $\Sigma$ -SC) DFT+DMFT scheme. For the correlated orbitals, i.e., those that acquire a Coulomb interaction in DMFT,  $\Sigma$ -SC DFT+DMFT takes the (linearized and Hermitianized) DMFT self-energy as the exchange-correlation potential in a similar way as proposed by Schilfgaarde and Kotani [40,41] for QS GW. That is, when solving the Kohn-Sham equation, these correlated orbitals sense the (linearized and Hermitianized) DMFT self-energy instead of the conventional LDA or GGA exchange-correlation potential. For the less correlated orbitals, that do not acquire an interaction in DMFT, the GGA is still employed. The method is self-consistent, for both electronic charge density and self-energy, avoiding the double-counting ambiguity. We employ the approach to SrVO<sub>3</sub> and find that it renders the correct position of the oxygen  $p$  orbitals. This indicates that using the Hermitianized DMFT self-energy provides a better Kohn-Sham potential for the correlated orbitals than conventional GGA potentials. A further advantage is that the “DFT” and “DMFT” parts of the calculation now show similar quasiparticle-renormalized spectra around the Fermi energy.

The outline of the paper is as follows: In Sec. II, we introduce the  $\Sigma$ -SC DFT+DMFT. In this section, we first recapitulate the conventional steps of DFT in Sec. II A, the projection onto Wannier functions in Sec. II B, and DMFT in Sec. II C. Carrying out these three steps constitutes a so-called one-shot DFT+DMFT calculation, whereas, as discussed in Sec. II D, in a CSC scheme the charge recalculated after the DMFT is fed back to the Kohn-Sham equation to obtain a new one-particle Kohn-Sham Hamiltonian until self-consistency is obtained. The decisive step of this paper, described in Sec. II E, is to take not only the charge but also the DMFT self-energy as the exchange-correlation potential of the correlated orbitals when going back to the Kohn-Sham equation after the DMFT step. The proper subtraction of the Hartree term to avoid a double counting is discussed in Sec. II F. An overview of the method in form of a flow diagram of the individual steps as well as of the full  $\Sigma$ -SC DFT+DMFT scheme is provided in Sec. II G and Fig. 1. Section III presents the results for SrVO<sub>3</sub> and SrRuO<sub>3</sub>, and Sec. IV a summary and outlook.

## II. METHODOLOGY

In this section, we present the formalism and implementation of self-energy self-consistency ( $\Sigma$ -SC). The actual implementation is based on the maximally localized Wannier functions (MLWF) and extends our previous CSC DFT+DMFT [25] implementation. Let us emphasize that the  $\Sigma$ -SC is a major improvement on the CSC: not only the charge but, based on the DMFT self-energy, also the exchange-correlation potential of the Kohn-Sham equations is changed. Specifically, our starting point is a DFT

calculation within WIEN2K [45], followed by a DMFT calculation which is performed with W2DYNAMICS [46] using continuous-time quantum Monte Carlo (CTQMC) [47] as an impurity solver. The identification of localized orbitals in DMFT is done with WIEN2WANNIER [48], an interface between WIEN2K [45] and WANNIER90 [49]. In  $\Sigma$ -SC, the self-consistency does not only include an update of the charge in the Kohn-Sham equation, but further modifies the exchange-correlation potential on the basis of the linearized DMFT self-energy. This step, distinguishing our work from previous DFT+DMFT implementations, is presented in Sec. II E. This way, genuine effects of electronic correlations are included in the exchange-correlation potential and a double counting is avoided.

### A. DFT cycle

Let us start by defining the central quantities of the  $\Sigma$ -SC DFT+DMFT: the electronic charge density as the key quantity in DFT and the Green's function (or the related self-energy) as the central component of DMFT. The charge density at a given spatial position  $\mathbf{r}$  is given by the equal-time Green's function or as a sum of all Matsubara frequency:

$$\rho(\mathbf{r}) = \frac{1}{\beta} \sum_n G(\mathbf{r}, \mathbf{r}; i\omega_n) e^{i\omega_n 0^+}, \quad (1)$$

while the local DMFT Green's function defined with localized Wannier orbitals  $\chi_m$  is given by

$$G_{mm'}(i\omega_n) = \int d\mathbf{r} d\mathbf{r}' \chi_m^*(\mathbf{r}) \chi_{m'}(\mathbf{r}') G(\mathbf{r}, \mathbf{r}'; i\omega_n). \quad (2)$$

Here  $m, m'$  denote the orbitals on the same site,  $\beta$  is the inverse temperature, and the convergence of the summation over Matsubara frequencies  $\omega_n = (2n + 1)\pi/\beta$  is ensured by the factor  $e^{i\omega_n 0^+}$ . The full Green's function for the solid appears in both equations and can be written as

$$G(\mathbf{r}, \mathbf{r}'; i\omega) = \langle \mathbf{r} | [i\omega_n + \mu - \hat{H}_{\text{KS}} - \Delta \hat{\Sigma}]^{-1} | \mathbf{r}' \rangle. \quad (3)$$

Here,  $\mu$  is the chemical potential and  $\hat{H}_{\text{KS}}$  the one-particle Hamiltonian of the Kohn-Sham equation consisting of the kinetic energy operator  $\hat{T}$  and the effective Kohn-Sham (KS) potential  $\hat{V}_{\text{KS}}$ .  $\Delta \hat{\Sigma} = \hat{\Sigma} - \hat{\Sigma}_{\text{dc}}$  is the effective local self-energy, where  $\hat{\Sigma}$  is the DMFT self-energy and  $\hat{\Sigma}_{\text{dc}}$  is the double-counting correction. In  $\Sigma$ -SC, the latter is determined explicitly, as detailed in Sec. II F. In a DFT calculation, the KS potential  $\hat{V}_{\text{KS}}$  has an explicit dependence on the total electronic charge  $\rho(\mathbf{r})$  and consists of an external potential  $\hat{V}_{\text{ion}}$  due to the nuclei (ions), a Hartree potential  $\hat{V}_H$ , describing the electron-electron Coulomb repulsion, and an exchange-correlation potential  $\hat{V}_{\text{xc}}$ , i.e.,  $\hat{V}_{\text{KS}} = \hat{V}_{\text{ext}} + \hat{V}_H + \hat{V}_{\text{xc}}$ . Altogether this yields

$$\hat{H}_{\text{KS}} = \hat{T} + \hat{V}_{\text{ext}} + \hat{V}_H + \hat{V}_{\text{xc}}. \quad (4)$$

There are several widely employed approximations of the latter term, such as using LDA [50], GGA [51], or hybrid functionals [52,53]. For our calculations on  $\Sigma$ -SC, we have employed GGA-PBE [51] but this is of little importance as the potential will be later replaced by a newly formulated one that is obtained from the self-energy  $\hat{\Sigma}$ .

The DFT self-consistency cycle (“DFT cycle”) hence consists of the following two steps: (i) The calculation of the exchange-correlation potential from the electronic charge distribution  $\rho(\mathbf{r}) \rightarrow V_{\text{KS}}(\mathbf{r})$ . (ii) The solution of the Kohn-Sham equation [written in Eq. (3) in form of a Green's function] and the recalculation of the charge [through Eq. (1)] provide together the second step  $V_{\text{KS}}(\mathbf{r}) \rightarrow \rho(\mathbf{r})$ .

### B. Wannier projection

Our starting point is a self-consistent DFT calculation with a converged electronic charge density. At this point,  $V_{\text{xc}}$  is calculated with GGA. The next step is to construct a localized orbital basis, which is required in DMFT that treats local correlations. For this purpose, we utilize MLWFs which can be obtained by taking a Fourier transformation of the DFT Bloch waves  $|\psi_{\mathbf{v}\mathbf{k}}\rangle$ :

$$|w_{\alpha\mathbf{R}}\rangle = \frac{\Omega}{(2\pi)^3} \int_{\text{BZ}} d\mathbf{k} e^{-i\mathbf{k}\mathbf{R}} \sum_{\nu=1}^{\mathcal{C}} U_{\nu\alpha}(\mathbf{k}) |\psi_{\nu\mathbf{k}}\rangle. \quad (5)$$

Here,  $\hat{U}(\mathbf{k})$  represents the (unitary) transformation matrix between the DFT Bloch states and the MLWFs.  $\nu(\alpha)$  denotes the band (orbital) indices of the Bloch waves (Wannier functions) and  $\Omega$  is the volume of the unit cell. It is to be noted that, here and in the following, hats denote matrices (operators) in the orbital indices.  $\mathcal{C}$  defines an isolated band window of Bloch waves that typically includes, e.g., the  $d$  or  $t_{2g}$  orbitals of a transition metal oxide or, as in our example below,  $t_{2g}$  plus oxygen  $p$  orbital. In the scheme of maximally localized Wannier functions [49], the spread (spatial extension) of the Wannier functions describing the DFT band structure in the given energy window is minimized, and  $\hat{U}(\mathbf{k})$  is obtained from this minimization.

In general, the target bands are “entangled” with other, less important bands, at least at a few  $\mathbf{k}$  points. That is, there exists an “outer” band window  $\mathcal{C}^o(\mathbf{k})$  that consists of more Bloch functions than the number of target bands, implying  $\mathcal{C}^o(\mathbf{k}) \geq \mathcal{C}$  at each  $\mathbf{k}$  point. These bands are projected out by a so-called “disentanglement” procedure:

$$|w_{\alpha\mathbf{R}}\rangle = \frac{\Omega}{(2\pi)^3} \int_{\text{BZ}} d\mathbf{k} e^{-i\mathbf{k}\mathbf{R}} \sum_{\nu=1}^{\mathcal{C}^o(\mathbf{k})} \sum_{\nu'=1}^{\mathcal{C}} V_{\nu\nu'}(\mathbf{k}) U_{\nu'\alpha}(\mathbf{k}) |\psi_{\nu\mathbf{k}}\rangle. \quad (6)$$

Here,  $\hat{V}(\mathbf{k})$  is a rectangular  $\mathcal{C}^o(\mathbf{k}) \times \mathcal{C}$  disentanglement matrix. The band indices  $\nu, \nu'$  label the bands in  $\mathcal{C}^o(\mathbf{k})$  and  $\mathcal{C}$ , respectively. Technically, it is advantageous to represent the Wannier orbitals in  $\mathbf{k}$  space, which is obtained with a Fourier transformation:

$$|w_{\alpha\mathbf{k}}\rangle = \sum_{\mathbf{R}} e^{i\mathbf{k}\mathbf{R}} |w_{\alpha\mathbf{R}}\rangle = \sum_{\nu\nu'} V_{\nu\nu'}(\mathbf{k}) U_{\nu'\alpha}(\mathbf{k}) |\psi_{\nu\mathbf{k}}\rangle \quad (7)$$

and the corresponding Wannier Hamiltonian is calculated:

$$\hat{H}_{\text{KS}}^{\mathcal{W}}(\mathbf{k}) = \hat{U}^\dagger(\mathbf{k}) \hat{H}_{\text{KS}}(\mathbf{k}) \hat{U}(\mathbf{k}), \quad (8)$$

$$\hat{H}_{\text{KS}}^{\mathcal{W}}(\mathbf{k}) = \hat{U}^\dagger(\mathbf{k}) \hat{V}^\dagger(\mathbf{k}) \hat{H}_{\text{KS}}(\mathbf{k}) \hat{V}(\mathbf{k}) \hat{U}(\mathbf{k}). \quad (9)$$

The two equations correspond to the case without and with disentanglement.

### C. DMFT cycle

The Hamiltonian is supplemented with a local Coulomb interaction, and the resulting lattice problem is solved in DMFT by mapping it onto an auxiliary impurity problem, which is solved self-consistently in DMFT [4,5]. Here, either the non-interacting Green's function  $\hat{G}(i\omega_n)$  of the impurity problem or the local self-energy can be considered as a dynamical mean field. The DMFT formalism consists of the following four steps: (i) The  $\mathbf{k}$ -integrated lattice Dyson equation yields the local interacting Green's function  $\hat{G}(i\omega_n)$ ,

$$\hat{G}(i\omega_n) = \frac{1}{n_{\mathbf{k}}} \sum_{\mathbf{k}} [i\omega_n + \mu - \hat{H}_{\text{KS}}^{\mathcal{W}}(\mathbf{k}) - \hat{\Sigma}(i\omega_n) + \hat{\Sigma}_{\text{dc}}]^{-1}, \quad (10)$$

from the local self-energy  $\hat{\Sigma}$  and one-particle Kohn-Sham Hamiltonian  $\hat{H}_{\text{KS}}^{\mathcal{W}}$ ;  $n_{\mathbf{k}}$   $\mathbf{k}$  points are considered in the reducible Brillouin zone. At this point, one usually starts with the Hartree energy as the first guess for  $\hat{\Sigma}$  for a faster convergence, which corresponds to  $\hat{\Sigma} = \hat{\Sigma}_{\text{dc}}$ . (ii) The impurity Dyson equation provides the noninteracting Green's function  $\hat{G}$  of the Anderson impurity model

$$\hat{G}(i\omega_n)^{-1} = \hat{\Sigma}(i\omega_n) + [\hat{G}(i\omega_n)]^{-1}. \quad (11)$$

(iii) Solving the Anderson impurity problem (AIM) defined by  $\hat{G}$  and the Coulomb interaction  $U$  gives interacting Green's function

$$\hat{G}(i\omega_n), U \xrightarrow{\text{AIM}} \hat{G}_{\text{imp}}(i\omega_n). \quad (12)$$

To this end, we employ the continuous-time quantum Monte Carlo method [47], as implemented in the w2DYNAMICS program package [46]. (iv) Applying the impurity Dyson equation a second time once again gives the self-energy

$$\hat{\Sigma}(i\omega_n) = \hat{G}^{-1}(i\omega_n) - \hat{G}_{\text{imp}}^{-1}(i\omega_n). \quad (13)$$

In the DMFT self-consistency cycle ("DMFT cycle"), the obtained self-energy is now used again in step (i) to recalculate a new local Green's function until a convergence is achieved. The "one-shot DFT+DMFT" ends after a full DFT cycle and one subsequent DMFT cycle. Physical quantities, e.g., spectral function, susceptibility, etc., are extracted at this point. Both in a charge CSC and  $\Sigma$ -SC DFT-DMFT one goes instead back to the DFT part as discussed in the following.

### D. Recalculation of the charge density

For the  $\Sigma$ -SC approach, we now go one step further. We construct a new electronic charge density (as has been done before) and a new exchange correlation potential for the correlated subspace. The total charge density is separable into two parts: (i) the correlated part  $\rho^c(\mathbf{r})$ , formed by the correlated orbitals (typically the  $d$  or  $f$  orbitals) and (ii) the noninteracting part  $\rho^{\text{rest}}(\mathbf{r})$ , formed by the rest of the system, i.e.,

$$\rho(\mathbf{r}) = \rho^c(\mathbf{r}) + \rho^{\text{rest}}(\mathbf{r}). \quad (14)$$

Including the DMFT correlations,  $\rho^c(\mathbf{r})$  can be calculated from the local DMFT Green's function as follows:

$$\rho^c(\mathbf{r}) = \frac{1}{n_{\mathbf{k}}} \sum_{\mathbf{k}, \alpha\alpha'} \langle \mathbf{r} | w_{\alpha\mathbf{k}} \rangle N_{\alpha\alpha'}^{\mathcal{W}}(\mathbf{k}) \langle w_{\alpha'\mathbf{k}} | \mathbf{r} \rangle. \quad (15)$$

Here,  $N_{\alpha\alpha'}^{\mathcal{W}}(\mathbf{k}) = \langle c_{\alpha\mathbf{k}}^\dagger c_{\alpha'\mathbf{k}} \rangle$  is the expectation value of the occupation operator in the localized Wannier orbitals basis  $\alpha, \alpha'$  which can be directly calculated from the equal time (or Matsubara sum) of the corresponding DMFT Green's function  $\hat{G}$ , which is again a matrix with respect to the orbitals. For a faster convergence of the Matsubara sum, it is advisable to express  $\hat{N}^{\mathcal{W}}$  as

$$\hat{N}^{\mathcal{W}}(\mathbf{k}) = \frac{1}{\beta} \sum_n [\hat{G}(\mathbf{k}, i\omega_n) - \hat{G}^*(\mathbf{k}, i\omega_n)] + \hat{f}(\mathbf{k}). \quad (16)$$

Here, the functional behavior of  $\hat{G}$  at higher frequency is considered by a model Green's function  $\hat{G}^*$ , and  $\hat{f}$  provides the analytical frequency sum of  $\hat{G}^*$ :

$$\hat{G}^*(\mathbf{k}, i\omega_n) = [i\omega_n - \hat{h}(\mathbf{k})]^{-1}, \quad (17)$$

$$\hat{h}(\mathbf{k}) = [-\mu + \hat{H}_{\text{KS}}^{\mathcal{W}}(\mathbf{k}) + \hat{\Sigma}(\infty) - \hat{\Sigma}^{\text{dc}}], \quad (18)$$

$$\hat{f}(\mathbf{k}) = \frac{1}{2} \left( 1 - \tanh \left[ \frac{\beta}{2} \hat{h}(\mathbf{k}) \right] \right). \quad (19)$$

Note that  $\hat{H}_{\text{KS}}^{\mathcal{W}}$  is, in general, not diagonal in Wannier representation. To calculate the analytical sum  $\hat{f}$ , we diagonalize  $\hat{h}(\mathbf{k})$ . If  $v_{\alpha i}$  is the  $i$ th eigenvector and  $w_i$  the  $i$ th eigenvalue of  $\hat{h}(\mathbf{k})$ , we get

$$\hat{f}'_i(\mathbf{k}) = \frac{1}{2} \left( 1 - \tanh \left[ \frac{\beta}{2} w_i(\mathbf{k}) \right] \right), \quad (20)$$

$$\hat{f}_{\alpha\alpha'}(\mathbf{k}) = v_{\alpha i} f'_i(\mathbf{k}) (v_{\alpha' i})^*. \quad (21)$$

The operator  $N^{\mathcal{W}}$  is then transformed to the Bloch basis utilizing the unitary and the disentanglement matrices  $\hat{U}(\mathbf{k})$  and  $\hat{V}(\mathbf{k})$ :

$$\hat{N}(\mathbf{k}) = \hat{U}(\mathbf{k}) \hat{N}^{\mathcal{W}}(\mathbf{k}) \hat{U}^\dagger(\mathbf{k}), \quad (22)$$

$$\hat{N}(\mathbf{k}) = \hat{V}(\mathbf{k}) \hat{U}(\mathbf{k}) \hat{N}^{\mathcal{W}}(\mathbf{k}) \hat{U}^\dagger(\mathbf{k}) \hat{V}^\dagger(\mathbf{k}). \quad (23)$$

From this, the correlated charge density is finally obtained as

$$\rho^c(\mathbf{r}) = \frac{1}{n_{\mathbf{k}}} \sum_{\mathbf{k}} \sum_{v v'=1}^{c^o} D_{v v'}^{\mathbf{k}}(\mathbf{r}) N_{v v'}(\mathbf{k}). \quad (24)$$

The remaining density  $\rho^{\text{rest}}(\mathbf{r})$  is calculated within DFT and added to  $\rho^c(\mathbf{r})$  to obtain the total electronic charge density.

### E. Recalculation of the exchange-correlation potential from the DMFT self-energy

The next step is the key aspect of the  $\Sigma$ -SC DFT+DMFT approach: recalculating the exchange-correlation potential for the next iteration step on the DFT side. The Hartree potential  $V_H(\mathbf{r})$  is calculated as usual from the total density, including the effect of electronic correlations on the density. The exchange-correlation (xc) potential for the next step is, however, not derived from the total charge density (e.g., using the GGA functional) as in previous CSC DFT+DMFT calculations. Instead, we split the xc potential into two parts:

$$\hat{V}_{\text{xc}}^{\text{DFT}} = \hat{V}_{\text{xc}}^c + \hat{V}_{\text{xc}}^{\text{rest}}. \quad (25)$$

Here,  $\hat{V}_{\text{xc}}^c$  corresponds to the xc potential for the correlated subspace and  $\hat{V}_{\text{xc}}^{\text{rest}}$  accounts for the xc of the rest of the system.

We now approximate these two xc potentials: We calculate  $\hat{V}_{xc}^{\text{DFT}}$  and  $\hat{V}_{xc}^c$  from the GGA xc potential at the corresponding densities  $\rho(\mathbf{r})$  and  $\rho^c(\mathbf{r})$ , respectively. This would yield exactly the same GGA xc potential if the charges are well separated, which is however hardly the case in practice.

From these, we obtain also the difference  $\hat{V}_{xc}^{\text{rest}} = \hat{V}_{xc}^{\text{DFT}} - \hat{V}_{xc}^c$ . This xc potential,  $\hat{V}_{xc}^{\text{rest}}$ , for the uncorrelated orbitals is the first part of our xc potential. The linearized and Hermitianized DMFT self-energy is added as the second part. Through the total xc potential  $\hat{V}_{xc}^{\text{DFT}}$  calculated from  $\rho(\mathbf{r})$ , it includes the core-valence interaction and the interaction between correlated and uncorrelated subspace. Even after subtraction of  $\hat{V}_{xc}^c$ ,  $\hat{V}_{xc}^{\text{rest}}$  will still possess that part of the interaction. Only the xc potential stemming from the interaction within the correlated subspace is taken out in  $\hat{V}_{xc}^{\text{rest}}$ . The aforementioned interaction part would be missing if the total charge density is divided between the correlated and the uncorrelated parts and potentials are calculated subsequently.

As every used xc potential,  $\hat{V}_{xc}^{\text{rest}}$  is an approximation for all xc contributions except for those in the correlated subspace. Similar subtractions of the  $d$  contributions to the exchange-correlation potential have been done before [33,34,54], but not the next step: using the DMFT self-energy instead of  $\hat{V}_{xc}^c$ .

That is, we employ a new xc potential within the correlated subspace  $\hat{\mathcal{V}}_{xc}^c$ , which is given by the (linearized and Hermitianized) DMFT self-energy  $\hat{\Sigma}$ . By construction,  $\hat{\Sigma}$  is local (in Wannier space) and represented in Matsubara frequencies. Because of this frequency dependence,  $\Sigma$  cannot be employed directly in the one-particle Kohn-Sham equation. But, one can take the real part of  $\hat{\Sigma}$  at the most relevant frequency  $\omega$  for every  $\mathbf{k}$  point which is  $\text{Re}\hat{\Sigma}(\omega = \epsilon_k)$ .

A further complication emerges from the fact that at least CTQMC calculation requires an analytical continuation for getting the self-energy at real frequencies. Maybe other approaches such as matrix-product states [55] can avoid these hassles in the future. For the time being this makes a direct implementation with  $\text{Re}\hat{\Sigma}(\omega = \epsilon_k)$  impractical.

However, as we focus on the low-energy part of the spectrum, we can linearize the self-energy around zero frequency

$$\hat{\Sigma}(\omega) \approx \hat{\Sigma}^{\text{lin}}(\omega) = \text{Re}\hat{\Sigma}(0) + \omega \left. \frac{\partial \hat{\Sigma}}{\partial \omega} \right|_{\omega=0}. \quad (26)$$

This linearized self-energy is still frequency dependent. Hence, it still cannot be included in the Kohn-Sham equation which is based on a frequency-independent Hamiltonian. But we can now use

$$\begin{aligned} \text{Re}\hat{\Sigma}(\omega = \epsilon_k) &\approx \hat{\Sigma}^{\text{lin}}(\omega = \epsilon_k) \\ &= \text{Re}\hat{\Sigma}(0) + [\epsilon_\alpha(\mathbf{k}) - \mu_{\text{DMFT}}] \left. \frac{\partial \hat{\Sigma}}{\partial \omega} \right|_{\omega=0}. \end{aligned} \quad (27)$$

That is, the  $\omega$  dependence of the DMFT self-energy matrix in Eq. (26) is replaced by a  $\mathbf{k}$  dependence in Eq. (27), taking  $\omega = \epsilon_\alpha(\mathbf{k})$  at the most important frequency, namely, the quasiparticle energy. This way we have obtained a Hermitian operator describing the self-energy at the quasiparticle energies.

On the technical side we can estimate the (constant plus) linear behavior as follows:

$$\text{Re}\hat{\Sigma}(0) = \text{Re}[\hat{\Sigma}(\omega_n \rightarrow 0^+)], \quad (28)$$

$$\left. \frac{\partial \text{Re}\hat{\Sigma}(\omega)}{\partial \omega} \right|_{\omega=0} = \left. \frac{\text{Im}[\hat{\Sigma}(i\omega_n)]}{\omega_n} \right|_{\omega_n \rightarrow 0}. \quad (29)$$

For the results below we take the limit  $\omega_n \rightarrow 0$  in Eq. (29) by simply considering the value at the lowest Matsubara frequencies, but more complicated fitting procedures may be taken.

We also have to take into account that the DMFT self-energy contains a Hartree contribution. This is to be subtracted from the xc potential since the same is already included in the effective KS potential, i.e.,

$$\hat{\Sigma}'^{\mathcal{W}}(\mathbf{k}) = \hat{\Sigma}^{\text{lin}}(\mathbf{k}) - \hat{\Sigma}^H. \quad (30)$$

Here, one can deduce the Hartree term of DMFT as

$$\Sigma_i^{H\uparrow} = U n_{i\downarrow} + \sum_{i'}^{i' \neq i} [(U - 2J)n_{i'\downarrow} + (U - 3J)n_{i'\uparrow}] \quad (31)$$

from the spin-orbital-resolved occupations  $n_{i'\uparrow}$  of the Wannier orbitals, and the equivalent formula for the opposite spin.

When we recalculate the Kohn-Sham states with the linearized DMFT self-energy, we need the exchange-correlation potential in real space  $\mathbf{r}$ . Hence, we now have to transform the (linearized) self-energy back to the Bloch basis utilizing the preobtained transformation matrices (the formulas are without and with disentanglement, respectively):

$$\hat{\Sigma}'(\mathbf{k}) = \hat{U}(\mathbf{k}) \hat{\Sigma}'^{\mathcal{W}}(\mathbf{k}) \hat{U}^\dagger(\mathbf{k}), \quad (32)$$

$$\hat{\Sigma}'(\mathbf{k}) = \hat{V}(\mathbf{k}) \hat{U}(\mathbf{k}) \hat{\Sigma}'^{\mathcal{W}}(\mathbf{k}) \hat{U}^\dagger(\mathbf{k}) \hat{V}^\dagger(\mathbf{k}). \quad (33)$$

Finally, the exchange-correlation potential within the correlated subspace can be written on a radial grid as

$$\mathcal{V}_{xc}^d(\mathbf{r}) = \frac{1}{n_{\mathbf{k}}} \sum_{\mathbf{k}} \sum_{\nu\nu'=1}^{c^o} D_{\nu\nu'}^{\mathbf{k}}(\mathbf{r}) \Sigma'(\mathbf{k})_{\nu\nu'}. \quad (34)$$

In the Kohn-Sham equation we henceforth employ the xc potential  $\hat{V}_{xc}^{\text{rest}} + \mathcal{V}_{xc}^d(\mathbf{r})$  or the following one-particle Hamiltonian instead of Eq. (4):

$$\hat{H}_{\text{KS}} = \hat{T} + \hat{V}_{\text{ext}} + \hat{V}_H + \hat{V}_{xc}^{\text{rest}} + \hat{\mathcal{V}}_{xc}^c. \quad (35)$$

## F. Exact double-counting subtraction

In the  $\Sigma$ -SC formalism, the part of the self-energy used as exchange correlation within the correlated subspace is now explicitly defined through Eq. (35). One can hence subtract this contribution exactly when calculating the DMFT Green's function in Eq. (10), simply by setting

$$\hat{\Sigma}^{\text{dc}}(\mathbf{k}) = \hat{\Sigma}^{\text{lin}}(\mathbf{k}), \quad (36)$$

where  $\hat{\Sigma}^{\text{lin}}(\mathbf{k})$  comes from the previous iteration. Let us remind the reader that the  $\mathbf{k}$  dependence of the double counting originates from the linearization process where we replaced approximately  $\omega \approx \epsilon_\alpha(\mathbf{k})$  when going from Eq. (26) to (27).

Let us note again that the Hartree term enters  $\hat{H}_{\text{KS}}$  only once in form of  $\hat{\Sigma}^H$  but not in  $\hat{\mathcal{V}}_{xc}^c$  thanks to the subtraction

in  $\hat{\Sigma}'^{\mathcal{W}}$  in Eq. (30); using  $\hat{\Sigma}^{\text{lin}}$  instead of  $\hat{\Sigma}'^{\mathcal{W}}$  for the double counting warranties that the Hartree term cancels for the self-energy.

In  $\Sigma$ -SC DFT+DMFT, the ambiguity of the double-counting term is hence avoided altogether. The correlated orbitals that acquire a Coulomb interaction in DMFT obtain a linearized  $\hat{\Sigma}'$  in the Kohn-Sham equation which is known exactly and can be hence subtracted as  $\hat{\Sigma}^{\text{dc}}$  when going back to the DMFT side.

This does not imply that we know the exact self-energy contribution  $\hat{\Sigma}_{\text{dc}}$  from say the GGA xc potential. Instead we have replaced the GGA xc potential by a self-energy xc potential for which we know this contribution. We replace one approximation (GGA) by another ( $\Sigma$ -SC) for the correlated subspace. One might view this as replacing the problem of determining  $\hat{\Sigma}_{\text{dc}}$  on the DMFT side by the problem of determining  $\hat{V}_{\text{xc}}^c$ . For the latter we can, however, take a well-defined density functional, which then altogether yields another xc approximation than the GGA. The big advantage is that we do on the Kohn-Sham and DMFT sides the same thing, or at least, the arguably closest thing possible. That is, we solve the Kohn-Sham as close as possible to the self-energy of the many-body problem. Whether this new xc potential works better or worse than conventional GGA+DMFT will be tested below.

Actually, after subtracting  $\hat{\Sigma}^{\text{dc}}$  in Eq. (10) not even the linearization approximation of the self-energy enters the DMFT Green's function any longer, but is replaced by the full, frequency-dependent DMFT self-energy. The linearization and including it as  $\hat{\mathcal{V}}_{\text{xc}}^c$  in the Kohn-Sham potential only serves the purpose that the Kohn-Sham wave functions and eigenvalues are adjusted to correlation effects included in the DMFT self-energy. On the DMFT side, the full self-energy is taken.

### G. Flow diagram of $\Sigma$ -SC DFT+DMFT

The full  $\Sigma$ -SC DFT+DMFT altogether involves the following steps, as also depicted schematically in Fig. 1:

(i) At first, we perform a DFT cycle (top left part of Fig. 1) i.e., we obtain a fully converged charge density within DFT in order to have a reasonable starting electronic structure. Subsequently, the target bands for the Wannier projection are identified. From the second iteration onwards in  $\Sigma$ -SC, we perform only one single DFT iteration to update the DFT Kohn-Sham Hamiltonian, i.e., only the green arrow in Fig. 1 (top left part) is followed without achieving the convergence of the charge density within DFT. The xc potential for the correlated subspace is supplemented with the one obtained from the DMFT self-energy as discussed in Sec. II E. For this step, we employ the modified WIEN2K program package.

(ii) We compute the MLWFs within the identified target subspace as explained in Eqs. (5)–(7); consequently, the Kohn-Sham Hamiltonian is transformed from Bloch basis to the Wannier basis following Eq. (8). To this end, we use the WIEN2WANNIER [48] and WANNIER90 [49] program packages.

(iii) A single DMFT iteration is performed in order to obtain the self-energy  $\hat{\Sigma}$ , local Green's function  $\hat{G}$ , and the DMFT chemical potential  $\mu$  corresponding to a fixed particle number. It needs to be noted that at this point  $\hat{\Sigma}^{\text{lin}}(\mathbf{k})$  is used as double-counting term and  $\mu$  is calculated accordingly. To

this end, we use the W2DYNAMICS [46] program package. In practice, it is beneficial to start  $\Sigma$ -SC with a converged DMFT self-energy. Hence, we perform a DMFT cycle (i.e., using both green and orange lines in bottom right part of Fig. 1) just like in a one-shot DFT+DMFT scheme. Furthermore, we also impose an under-relaxation, i.e., a mixing between old and new DMFT self-energies for a well-behaved convergence.

(iv) The correlated charge distribution as well as the xc potential are updated (bottom left part of Fig. 1). At first,  $\hat{N}^{\mathcal{W}}(\mathbf{k})$  is calculated from the DMFT Green's functions  $\hat{G}$  as in Eq. (16).  $\hat{N}^{\mathcal{W}}(\mathbf{k})$  is then transformed back to the Bloch basis, as described in Eqs. (22) and (23) in order to calculate the correlated charge density  $\rho^c(\mathbf{r})$  in real space.

In a similar fashion, the xc potential  $\hat{\mathcal{V}}_{\text{xc}}^c$  in the correlated subspace is calculated from the DMFT self-energy through Eq. (30) and transformed back to DFT eigenbasis as presented in Eqs. (32), on a radial grid by employing Eq. (34).

(v) At the last step, the new total charge density (including DMFT density correction) is checked for convergence. If the convergence criterion is not achieved, we proceed with a new charge density which is again a mixture of the calculated new and the old charge density from the previous iteration. The charge density of the correlated orbitals  $\rho^c(\mathbf{r})$  is used to calculate  $\hat{V}_{\text{xc}}^c$ , which then provides  $\hat{V}_{\text{xc}}^{\text{rest}}$  as described in Eq. (25). The exchange correlation potential in the KS Hamiltonian is updated with  $\hat{V}_{\text{xc}}^{\text{rest}}$  and  $\hat{\mathcal{V}}_{\text{xc}}^c$  according to Eq. (35). At this step, the DMFT self-energy is also compared for two consecutive iterations for convergence so that we obtain a simultaneous convergence of both the quantities: total charge density and the local DMFT self-energy.

For the SrVO<sub>3</sub> calculations shown below, we needed about 60–70 iterations to converge, which might be sped up by a less cautious mixing (we only mixed in 20% of the new solution for the charge density and 30% of the new self-energy).

## III. RESULTS

The  $\Sigma$ -SC DFT+DMFT scheme is applied to SrVO<sub>3</sub>, a test-bed material for methodological developments for strongly correlated electron systems. The cubic perovskite structure of SrVO<sub>3</sub> results in degenerate  $t_{2g}$  bands near Fermi energy that are singly occupied and unoccupied  $e_g$  bands. Bulk SrVO<sub>3</sub> exhibits a strongly correlated metallic behavior and the electronic features are mostly governed by partially filled  $t_{2g}$  bands. In DFT+DMFT schemes, one typically treats isolated  $t_{2g}$  bands with explicit electron correlation in DMFT, coined as “ $d$ -only” model. As a consequence of the DMFT correlations, the wide band of DFT is renormalized by a factor of about 0.5, yielding a strongly correlated metal. Additional lower and upper Hubbard peaks appear at  $-1.7$  and  $2.5$  eV, respectively (see, e.g., Refs. [56–60] for previous DFT+DMFT calculations. In the energy range of the latter, also the  $e_g$  bands are located. The agreement of the  $t_{2g}$  spectral function with experiment is reasonably good [56]. SrVO<sub>3</sub> has also been studied in GW+DMFT by various groups [38,39,61–64]. GW+DMFT yields a somewhat better position of the lower Hubbard band [39,62,63] but does not fully solve the problem with the wrong position of the oxygen  $p$  bands [38,39,63], while improving the DFT+DMFT results.

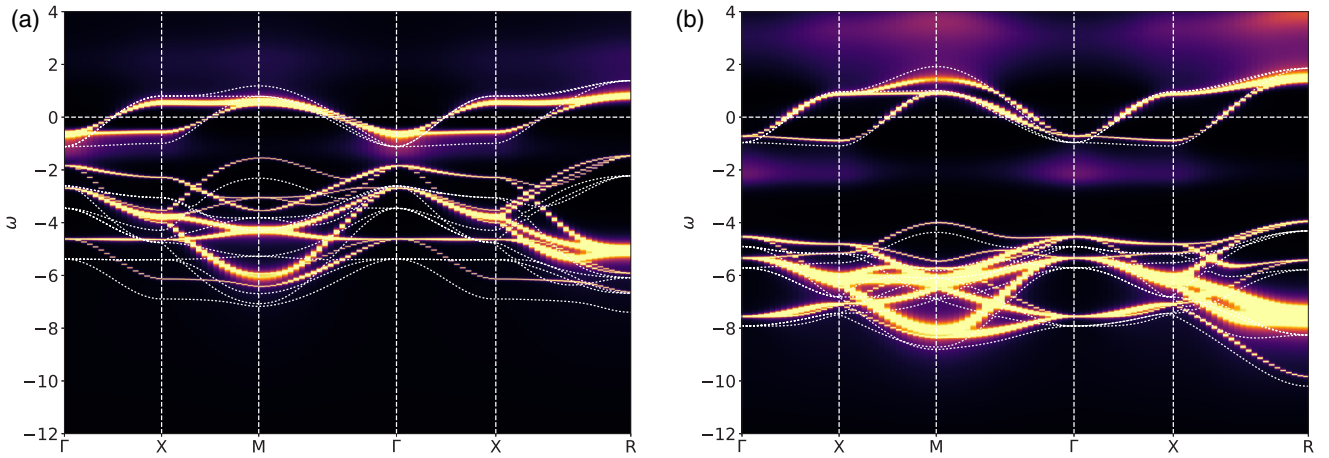


FIG. 2. (a) One-shot DFT+DMFT for SrVO<sub>3</sub> at  $U_{dd} = 9.5$  eV and  $J_{dd} = 0.75$  eV. The  $\mathbf{k}$ -dependent spectral function is plotted together with the DFT band structure (white dotted lines) along high-symmetry lines of the Brillouin zone. (b) Same as (a) but now with  $\Sigma$ -SC and the DFT band structure (white dotted lines) is obtained from the linearized DMFT self-energy at self-consistency. Note that the DFT band structure nicely follows the DMFT spectral function at low frequencies.

One can include noninteracting  $p$  bands within DMFT in a so-called “ $d+p$ ” calculation. However, the energy difference between  $d$  and  $p$  bands derived *ab initio* in DFT is underestimated. Consequently, there is a too strong hybridization between  $d$  and  $p$  orbitals, and the effective  $p$  orbitals have a significant  $d$  contribution. This in turn means that the  $d$  occupation is much larger than one. A  $d+p$  calculation with interaction in the  $t_{2g}$  bands and no interaction in the uncorrelated  $p$  bands hence yields only a weakly correlated solution with too wide  $t_{2g}$  bands around the Fermi energy and no Hubbard bands [24,26–31]. It is to be noted that, here and later in the case of SrRuO<sub>3</sub>, we refer to these calculations generically as “ $d+p$ ” instead of the more specialized term “ $t_{2g}+p$ .”

A  $d-p$  interaction [26], a GW correction [65], or an *ad hoc* “double-counting” term [31,32], which corrects the onsite energies of the  $p$  orbitals to the experimental position, needs to be introduced in order to obtain a proper Hubbard peak below the Fermi energy, as observed in experiment. Let us note that the origin of this peak has been debated. Namely, within a GW+extended DMFT calculation [64] it has been identified as a plasmon peak, which is, however, much less pronounced than in experiment, while Backes *et al.* [66] identified it coming from oxygen vacancy in a GW+DMFT framework. Altogether, this leaves  $d+p$  DFT+DMFT calculations in a quite unsatisfactory state, relying on parameter tuning or *ad hoc* corrections of the  $p$  level or exchange-correlation potential for getting the correct position of the oxygen  $p$  levels.

In our implementation, we employ instead the DMFT self-energy as the (self-consistently updated) exchange-correlation potential for the  $t_{2g}$  orbitals of SrVO<sub>3</sub>. That is, the GGA potential is only used for the less correlated oxygen  $p$  orbitals, whereas for the correlated, localized  $t_{2g}$  orbitals the local DMFT self-energy from a  $d+p$  calculation is used. In principle, this DMFT potential should also be employed for the  $e_g$  orbitals, but since these are essentially unoccupied, the DMFT self-energy would reduce to a Hartree term which is included in the GGA as well.

In Fig. 2(a), we first present the  $\mathbf{k}$ -dependent spectral function of SrVO<sub>3</sub> as obtained in a  $d+p$  model within a standard one-shot DFT+DMFT calculation, using  $U_{dd} = 9.5$  eV,  $J_{dd} = 0.75$  eV, zero  $U_{dp}$  and  $U_{pp}$ , and room temperature ( $\beta = 40$ ). Fully localized limit (FLL) double-counting term is considered here. Let us note that within a  $d+p$  model the impurity orbitals are more localized compared to those in a  $d$ -only model, causing larger values of the interaction parameters than in  $d$ -only calculation. The specific values are chosen following Aryasetiawan *et al.* [67] and will be considered for all the calculations presented in this paper.

The band renormalization is reasonable with  $Z \sim 0.48$ . However, the  $p$  bands appear around  $-2$  to  $-7$  eV, which does not agree with the experimental photoemission spectra [56,68–70]. As explained before, the  $p$  bands have to be adjusted to describe photoemission spectra. In SrVO<sub>3</sub>, the required shift is as large as  $\sim 5.0$  eV [32], which combined with the large  $U_{dd}$  (9.5 eV) of Ref. [67] would even result in an insulating solution.

Next, we turn to the  $\Sigma$ -SC DFT+DMFT, which does not necessitate such an *ad hoc* shift and treats SrVO<sub>3</sub> in a completely *ab initio* manner. As mentioned in Sec. II, we started from a converged one-shot DFT+DMFT self-energy [i.e., from the solution of Fig. 2(a)]. Upon  $\Sigma$ -SC self-consistency we however obtain the solution Fig. 2(b).

With the linearized DMFT self-energy as an input, the Kohn-Sham equations in the DFT part of the loop now reproduce the DMFT spectral function very well, which is not the case in one-shot calculations [Fig. 2(a)] or conventional CSC DFT+DMFT calculations. This is not surprising since the Kohn-Sham equations in the  $\Sigma$ -SC DFT+DMFT are especially adjusted to the electronic correlations. Indeed, the only difference between the DMFT self-energy on the DMFT side and the DMFT-derived exchange-correlation functional on the Kohn-Sham side is the linearization procedure.

There are deviations between the DFT band structure and the DMFT spectrum at larger frequencies, where we are simply outside the linear regime of the self-energy. Further,

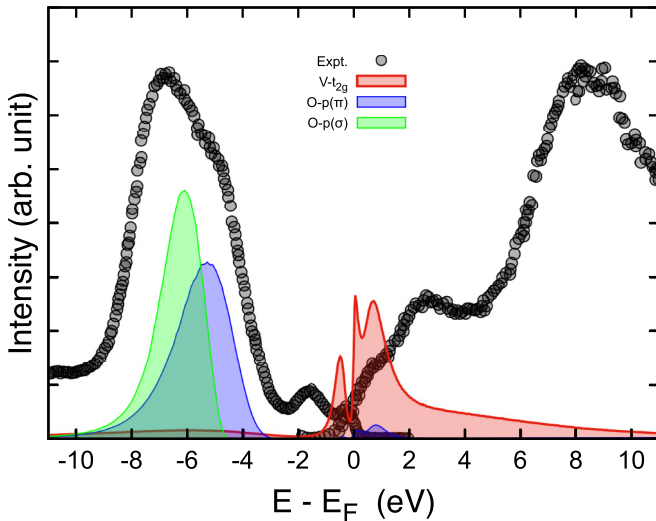


FIG. 3. Comparison of calculated spectral function and experimental photoemission spectra (PES) by Morikawa *et al.* [68]. The black circles and dots present experimental results. The red filled curve represents  $V-t_{2g}$  spectra while the blue and green curves correspond to O  $2p$ .  $U_{dd} = 9.5$  eV and  $J_{dd} = 0.75$  eV.

the DMFT spectral function shows (hardly visible) Hubbard bands which lead to a different chemical potential. With more complicated, e.g., piecewise-linear, forms of the self-energy exchange-correlation potential, one should be able to remedy this in the future. But we do not expect that the actual physical quantity, i.e., the DMFT spectral function, will be affected by this strongly.

Let us now turn to the position of the  $p$  bands relative to those of the  $t_{2g}$  bands. They are shifted to much lower energies. Now the oxygen  $p$  positions, without any adjustable parameters (as  $U$  is obtained from Ref. [67]) much better agree with the experimental spectra (see, e.g., Fig. 3). Please note that now, with  $\Sigma$ -SC the Kohn-Sham and DMFT  $p$  bands agree very well. In addition, interestingly, over the iteration in  $\Sigma$ -SC, also the dispersion of the  $p$  bands is slightly changed compared to that in DFT.

The scenario can be further clarified by inspecting the  $\mathbf{k}$ -integrated spectral function, Fig. 3, which compares our  $\Sigma$ -SC spectra with photoemission spectroscopy (PES) by Morikawa *et al.* [68]. In Fig. 3, the lower and upper Hubbard peaks are not very well pronounced in  $\Sigma$ -SC DFT+DMFT. They or reminiscences thereof are however present, and can also be seen as purple shades at around  $-2$  and  $+3.5$  eV in Fig. 2(b). These positions of the Hubbard bands agree with the PES spectrum. But the weight is smaller. In this respect, please keep in mind that more bulk-sensitive PES [56] has a larger weight in the quasiparticle peak than in the lower Hubbard band, similar but not as pronounced as in our  $\Sigma$ -SC DFT+DMFT calculation. One possible explanation for the less pronounced Hubbard peaks is the effective interaction  $U$  which we have taken from the literature [67]. Adjusting  $U$  to slightly larger values would yield more pronounced Hubbard bands. Indeed, when determining  $U$  self-consistently using  $\Sigma$ -SC DFT+DMFT we expect a larger  $U$  value, simply because the oxygen  $p$  orbitals are (correctly) pushed further away the

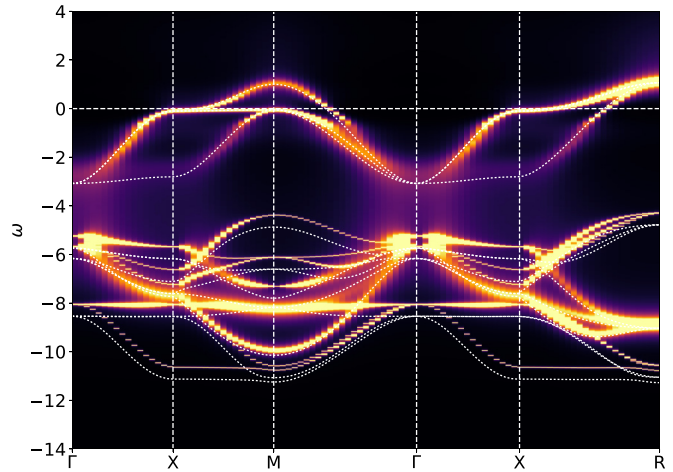


FIG. 4.  $\Sigma$ -SC DFT+DMFT for SrRuO<sub>3</sub> at  $U_{dd} = 5.0$  eV,  $J_{dd} = 0.55$  eV, and  $\beta = 40$ . The  $\mathbf{k}$ -integrated spectral function is plotted with the DFT band structure (white dotted lines), obtained from the linearized DMFT self-energy at self-consistency. Note that the DFT band structure nicely follows the DMFT spectral function at low frequencies.

$t_{2g}$  orbitals and hence become less effective in screening. But, such a self-consistency also with respect to  $U$  is beyond the scope of this paper.

Let us also note that there is additional spectral weight of the  $e_g^\sigma$  orbitals (not included in our calculations as these are unoccupied) which should be located slightly above our upper Hubbard band, as was already discussed in the very first DFT+DMFT calculations [56]. Further, spectral weight contributions from plasmon peaks [64] and impurities [66] are also discussed.

The main improvement with respect to previous DFT+DMFT calculations is that we also obtain an excellent description of the position of the oxygen  $p$  orbitals without any adjustable parameter or *ad hoc*  $p$ - $d$  shift. This includes their width and relative weight to the  $t_{2g}$  bands and, in particular, their splitting into two subgroups of oxygen  $p$  orbitals: out of nine orbitals the first branch [O  $p(\pi)$ ] consists of six orbitals with a peak at  $-5.0$  eV while the rest [O  $p(\sigma)$ ] are peaked at  $-6.1$  eV. A substantial shift of the  $p$  orbitals in the right direction has already been obtained when taking out the  $d$ -electron contribution from the exchange correlation potential [33,34,54]. But replacing it by the DMFT self-energy in  $\Sigma$ -SC DFT+DMFT is not only more appealing from a fundamental point of view, it also gives a much larger shift which is needed to obtain the correct (experimental) oxygen position.

We now apply our method to another perovskite material, SrRuO<sub>3</sub>. The  $\Sigma$ -SCDFT+DMFT is performed with interaction parameters  $U_{dd} = 5.0$  eV,  $J_{dd} = 0.55$  eV at room temperature ( $\beta = 40$ ).<sup>1</sup> The Ru  $t_{2g}$  bands show a wider dispersion. Concomitantly, the renormalization in  $\Sigma$ -SC is slightly less pronounced with  $Z \sim 0.64$ , in comparison with the  $V-t_{2g}$  bands in SrVO<sub>3</sub>. In Fig. 4, we show the  $\mathbf{k}$ -dependent spectral

<sup>1</sup>The interaction parameters are smaller for  $4d$  Ru than for  $3d$  V.



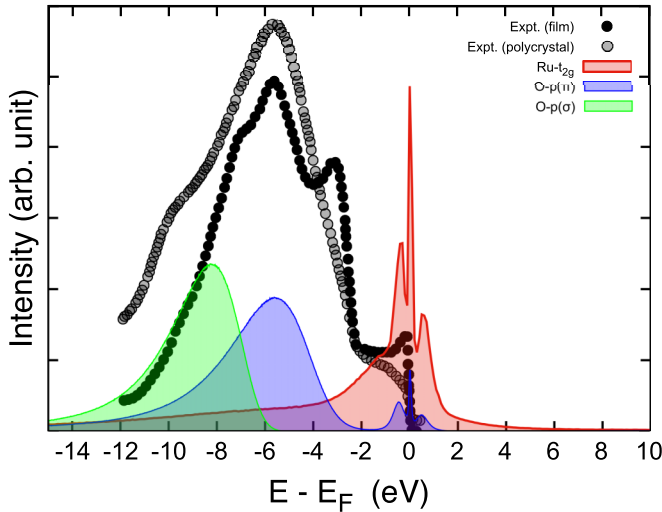


FIG. 5. Comparison of calculated spectral function and experimental ultraviolet photoemission spectra (UPS) by Kim *et al.* [71]. The black circles and dots represent experimental results corresponding to the scrapped surface of polycrystal and single-crystal thin film, respectively. The red filled curve represents Ru  $t_{2g}$  spectra while the blue and green curves correspond to O  $2p$ .  $U_{dd} = 5$  eV and  $J_{dd} = 0.55$  eV.

function, obtained in  $\Sigma$ -SC. The occupied  $t_{2g}$  bands span down to  $\sim 3$  eV below the Fermi energy, in good agreement with the experimental observation of  $\sim 2.5$  eV [71], which is further elucidated later with the  $\mathbf{k}$ -integrated spectra. At low energy, the DFT and the DMFT bands match well due to the linearized (and Hermitianized) self-energy within DFT, as also observed in the case of SrVO<sub>3</sub>. The crucial improvements of  $\Sigma$ -SC are seen in the energy positions of the O  $p$  bands. In  $\Sigma$ -SC, we find the spectral gap between  $t_{2g}$  and O  $p$  amounts to  $\sim 1.5$  eV, placing O  $p$  bands in the energy range between  $\sim 4.5$  and 11.0 eV below the Fermi energy. In a one-shot DFT+DMFT calculation (not shown), this gap is highly underestimated and is almost nonexistent.

To further elucidate the importance of  $\Sigma$ -SC, in Fig. 5, we compare the  $\mathbf{k}$ -integrated spectra with the reported experimental ultraviolet photoemission spectra (UPS) [71], obtained with single-crystal film (solid black dots) as well as the scrapped surface of polycrystal (empty circles). The Ru  $t_{2g}$  peaks, comprising of the coherent and the incoherent components, in both the experimental spectra appear within  $\sim 2.5$  eV energy range below Fermi level. In  $\Sigma$ -SC the  $t_{2g}$  spectra (red filled curve) span down to  $-3.0$  eV below the Fermi energy, including a relatively broad incoherent peak around  $\sim -1.35$  eV. Both the incoherent peak position and the  $t_{2g}$  bandwidth agree well with the experimental findings of  $-1.3$  and  $-2.5$  eV, respectively [71]. Importantly, the spectral gap between the O  $p$  and Ru  $t_{2g}$  is quite accurately reproduced in  $\Sigma$ -SC. The first O  $p$  ( $\pi$ ) peak (blue filled curve) appears around  $-5.0$  eV and the second, O  $p$  ( $\sigma$ ) peak (green filled curve) around  $-8.2$  eV. In the spectrum for the SrRuO<sub>3</sub> film, an additional peak is present at  $-3$  eV which along with the second O  $p$  peak at  $-7.5$  eV is absent in the spectrum for the scrapped surface of polycrystal. The peak at  $-3$  eV is identified as the O  $2p$  nonbonding state, which can be stemming

from the surface effect [72]. A similar behavior can also be observed in the PES spectra for SrVO<sub>3</sub> [68,69].

#### IV. SUMMARY AND OUTLOOK

We have introduced the  $\Sigma$ -SC DFT+DMFT method which avoids the double-counting problem, and employed it to SrVO<sub>3</sub> and SrRuO<sub>3</sub>. It yields largely improved results, in particular with regard to the position of the oxygen  $p$  bands, which has been a major shortcoming of previous DFT+DMFT calculations. Also, the Kohn-Sham bands now closely resemble the DMFT quasiparticle bands.

The essential step is to take the DMFT self-energy as the exchange-correlation potential of the correlated orbitals in the Kohn-Sham equation of the ‘‘DFT step.’’ As the latter is a one-particle equation, we must employ a Hermitianized and linearized self-energy at the proper quasiparticle energy in a similar manner as in QSGW [40,41].

However, when going back to the DMFT step this self-energy is readily replaced by the correct, frequency-dependent DMFT self-energy, using the many-body Dyson equation. Hence, solving the Kohn-Sham equations with the linearized self-energy can be seen as an intermediate step, only to adjust the one-particle orbitals to the actuality of electronic correlations. Thereafter, the self-energy with its full frequency dependence is taken again.

This is not fully correct since for the less correlated orbitals we still take the plain vanilla GGA potential of DFT. One might be tempted to extend the correlated subspace to all orbitals, using a DMFT self-energy also for these. Indeed, this is what is done in QSGW. However, we believe that in contrast to the QSGW this is not adequate for  $\Sigma$ -SC DFT+DMFT since the local DMFT self-energy should only provide a proper exchange-correlation potential for the more localized orbitals, typically the  $d$  or  $f$  orbitals of a transition metal oxide, lanthanide, or actinide. For these orbitals the local correlations as described in DMFT are prevalent. For the more extended, e.g.,  $p$  orbitals, on the other hand the exchange part is more important. This can be described to a large extent by the GGA, at least for metals, but not in DMFT.

Using a combination of DMFT self-energy for the correlated orbitals and GW for the less correlated orbitals, and feeding both back to the Kohn-Sham equation in a linearized form is at least appealing, and possibly even better than  $\Sigma$ -SC DFT+DMFT method, pending extensive further implementations and examination which are beyond the scope of this paper. An even further step is to include also nonlocal correlations beyond GW which is possible using the *ab initio* dynamical vertex approximation (D $\Gamma$ A) [73–75], and to feed the obtained nonlocal self-energy back to the Kohn-Sham equation in the same way as we do in this paper for the local DMFT self-energy.

The decisive step has been, however, already done in this paper, using a linearized DMFT-like self-energy in the Kohn-Sham equation. In other words, we calculate and readjust the Kohn-Sham states so that these most closely resemble the correlated DMFT spectrum. In our paper we have shown that this  $\Sigma$ -SC DFT+DMFT method does not only work properly, but also yields largely improved results compared to previous  $d+p$  calculations.

## ACKNOWLEDGMENTS

We thank J. Kaufmann for his devoted support regarding the maximum entropy analytical continuation; M. Aichhorn, E. Assmann, and P. Blaha for scientific discussions on implementing charge self-consistency in WIEN2K. This work has been supported by the European Research Council under

the European Union's Seventh Framework Programme (Grant No. FP/2007-2013)/ERC Grant Agreement No.. 306447 (*Ab initio* DΓA). S.B. acknowledges the support of Science Foundation Ireland (Grant No. 19/EPSC/3605) and the Engineering and Physical Sciences Research Council (Grant No. EP/S030263/1). The computational results presented have been achieved using the Vienna Scientific Cluster (VSC).

- 
- [1] W. Kohn, *Rev. Mod. Phys.* **71**, 1253 (1999).
- [2] R. O. Jones and O. Gunnarsson, *Rev. Mod. Phys.* **61**, 689 (1989).
- [3] W. Metzner and D. Vollhardt, *Phys. Rev. Lett.* **62**, 324 (1989).
- [4] A. Georges and G. Kotliar, *Phys. Rev. B* **45**, 6479 (1992).
- [5] A. Georges, G. Kotliar, W. Krauth, and M. Rozenberg, *Rev. Mod. Phys.* **68**, 13 (1996).
- [6] V. I. Anisimov, A. I. Poteryaev, M. A. Korotin, A. O. Anokhin, and G. Kotliar, *J. Phys.: Condens. Matter* **9**, 7359 (1997).
- [7] A. I. Lichtenstein and M. I. Katsnelson, *Phys. Rev. B* **57**, 6884 (1998).
- [8] K. Held, I. A. Nekrasov, G. Keller, V. Eyert, N. Blümer, A. K. McMahan, R. T. Scalettar, T. Pruschke, V. I. Anisimov, and D. Vollhardt, *Phys. Status Solidi B* **243**, 2599 (2006), previously appeared as Psi-k Newsletter No. 56 (2003).
- [9] G. Kotliar, S. Y. Savrasov, K. Haule, V. S. Oudovenko, O. Parcollet, and C. A. Marianetti, *Rev. Mod. Phys.* **78**, 865 (2006).
- [10] K. Held, *Adv. Phys.* **56**, 829 (2007).
- [11] V. Anisimov, F. Aryasetiawan, and A. I. Lichtenstein, *J. Phys.: Condens. Matter* **9**, 767 (1997).
- [12] K. Held, G. Keller, V. Eyert, D. Vollhardt, and V. I. Anisimov, *Phys. Rev. Lett.* **86**, 5345 (2001).
- [13] S. Bhandary, M. Schüler, Patrik Thunström, I. di Marco, B. Brena, O. Eriksson, T. Wehling, and B. Sanyal, *Phys. Rev. B* **93**, 155158 (2016).
- [14] J. Steinbauer, S. Biermann, and S. Bhandary, *Phys. Rev. B* **100**, 245418 (2019).
- [15] S. K. Panda, I. Di Marco, O. Granäs, O. Eriksson, and J. Fransson, *Phys. Rev. B* **93**, 140101(R) (2016).
- [16] S. Y. Savrasov, G. Kotliar, and E. Abrahams, *Nature (London)* **410**, 793 (2001).
- [17] K. Held, A. K. McMahan, and R. T. Scalettar, *Phys. Rev. Lett.* **87**, 276404 (2001).
- [18] S. Y. Savrasov and G. Kotliar, *Phys. Rev. B* **69**, 245101 (2004).
- [19] J. Minár, L. Chioncel, A. Perlov, H. Ebert, M. I. Katsnelson, and A. I. Lichtenstein, *Phys. Rev. B* **72**, 045125 (2005).
- [20] H. Park, A. J. Millis, and C. A. Marianetti, *Phys. Rev. B* **90**, 235103 (2014).
- [21] F. Lechermann, A. Georges, A. Poteryaev, S. Biermann, M. Posternak, A. Yamasaki, and O. K. Andersen, *Phys. Rev. B* **74**, 125120 (2006).
- [22] L. V. Pourovskii, B. Amadon, S. Biermann, and A. Georges, *Phys. Rev. B* **76**, 235101 (2007).
- [23] M. Aichhorn, L. Pourovskii, and A. Georges, *Phys. Rev. B* **84**, 054529 (2011).
- [24] K. Haule, C.-H. Yee, and K. Kim, *Phys. Rev. B* **81**, 195107 (2010).
- [25] S. Bhandary, E. Assmann, M. Aichhorn, and K. Held, *Phys. Rev. B* **94**, 155131 (2016).
- [26] P. Hansmann, N. Parragh, A. Toschi, G. Sangiovanni, and K. Held, *New J. Phys.* **16**, 033009 (2014).
- [27] K. Held, <http://online.kitp.ucsb.edu/online/cem02/held>.
- [28] X. Wang, M. J. Han, L. de' Medici, H. Park, C. A. Marianetti, and A. J. Millis, *Phys. Rev. B* **86**, 195136 (2012).
- [29] K. Haule, T. Birol, and G. Kotliar, *Phys. Rev. B* **90**, 075136 (2014).
- [30] N. Parragh, G. Sangiovanni, P. Hansmann, S. Hummel, K. Held, and A. Toschi, *Phys. Rev. B* **88**, 195116 (2013).
- [31] H. T. Dang, A. J. Millis, and C. A. Marianetti, *Phys. Rev. B* **89**, 161113(R) (2014).
- [32] Z. Zhong, M. Wallerberger, J. M. Tomczak, C. Taranto, N. Parragh, A. Toschi, G. Sangiovanni, and K. Held, *Phys. Rev. Lett.* **114**, 246401 (2015).
- [33] I. A. Nekrasov, N. S. Pavlov, and M. V. Sadovskii, *JETP Lett.* **95**, 581 (2012).
- [34] I. A. Nekrasov, N. S. Pavlov, and M. V. Sadovskii, *JETP* **116**, 620 (2013).
- [35] L. Hedin, *Phys. Rev.* **139**, A796 (1965).
- [36] S. Biermann, F. Aryasetiawan, and A. Georges, *Phys. Rev. Lett.* **90**, 086402 (2003).
- [37] P. Sun and G. Kotliar, *Phys. Rev. B* **66**, 085120 (2002).
- [38] J. M. Tomczak, P. Liu, A. Toschi, G. Kresse, K. Held, *Eur. Phys. J.: Spec. Top.* **226**, 2565 (2017).
- [39] J. M. Tomczak, M. Casula, T. Miyake, F. Aryasetiawan, and S. Biermann, *Europhys. Lett.* **100**, 67001 (2012).
- [40] S. V. Faleev, M. van Schilfgaarde, and T. Kotani, *Phys. Rev. Lett.* **93**, 126406 (2004).
- [41] A. N. Chantis, M. van Schilfgaarde, and T. Kotani, *Phys. Rev. Lett.* **96**, 086405 (2006).
- [42] J. M. Tomczak, M. van Schilfgaarde, and G. Kotliar, *Phys. Rev. Lett.* **109**, 237010 (2012).
- [43] J. M. Tomczak, *J. Phys.: Conf. Ser.* **592**, 012055 (2015).
- [44] D. Jacob, K. Haule, and G. Kotliar, *Europhys. Lett.* **84**, 57009 (2008).
- [45] P. Blaha, K. Schwarz, G. K. H. Madsen, D. Kvasnicka, J. Luitz, *WIEN2k, An Augmented Plane Wave + Local Orbitals Program for Calculating Crystal Properties* (Karlheinz Schwarz, Techn. Universitat Wien, Austria, 2001).
- [46] N. Parragh, A. Toschi, K. Held, and G. Sangiovanni, *Phys. Rev. B* **86**, 155158 (2012); M. Wallerberger, A. Hausoel, P. Gunacker, A. Kowalski, N. Parragh, F. Goth, K. Held, and G. Sangiovanni, *Comput. Phys. Commun.* **235**, 388 (2019).
- [47] E. Gull, A. J. Millis, A. I. Lichtenstein, A. N. Rubtsov, M. Troyer, and P. Werner, *Rev. Mod. Phys.* **83**, 349 (2011).
- [48] J. Kunes, R. Arita, P. Wissgott, A. Toschi, H. Ikeda, and K. Held, *Comput. Phys. Commun.* **181**, 1888 (2010).
- [49] A. A. Mostofi, J. R. Yates, Y.-S. Lee, I. Souza, D. Vanderbilt, and N. Marzari, *Comput. Phys. Commun.* **178**, 685 (2008).

- [50] W. Kohn and L. J. Sham, *Phys. Rev.* **140**, A1133 (1965).
- [51] J. P. Perdew, K. Burke, and M. Ernzerhof, *Phys. Rev. Lett.* **77**, 3865 (1996); **78**, 1396(E) (1997).
- [52] F. Tran and P. Blaha, *Phys. Rev. Lett.* **102**, 226401 (2009).
- [53] A. D. Becke, *J. Chem. Phys.* **98**, 5648 (1993).
- [54] K. Haule, *Phys. Rev. Lett.* **115**, 196403 (2015).
- [55] F. A. Wolf, I. P. McCulloch, and U. Schollwöck, *Phys. Rev. B* **90**, 235131 (2014); M. Ganahl, P. Thunström, F. Verstraete, K. Held, and H. G. Evertz, *ibid.* **90**, 045144 (2014); D. Bauernfeind, R. Triebl, M. Zingl, M. Aichhorn, and H. G. Evertz, *ibid.* **97**, 115156 (2018).
- [56] A. Sekiyama, H. Fujiwara, S. Imada, S. Suga, H. Eisaki, S. I. Uchida, K. Takegahara, H. Harima, Y. Saitoh, I. A. Nekrasov, G. Keller, D. E. Kondakov, A. V. Kozhevnikov, Th. Pruschke, K. Held, D. Vollhardt, and V. I. Anisimov, *Phys. Rev. Lett.* **93**, 156402 (2004).
- [57] E. Pavarini, S. Biermann, A. Poteryaev, A. I. Lichtenstein, A. Georges, and O. K. Andersen, *Phys. Rev. Lett.* **92**, 176403 (2004).
- [58] A. Liebsch, *Phys. Rev. Lett.* **90**, 096401 (2003).
- [59] I. A. Nekrasov, G. Keller, D. E. Kondakov, A. V. Kozhevnikov, T. Pruschke, K. Held, D. Vollhardt, and V. I. Anisimov, *Phys. Rev. B* **72**, 155106 (2005).
- [60] I. A. Nekrasov, K. Held, G. Keller, D. E. Kondakov, T. Pruschke, M. Kollar, O. K. Andersen, V. I. Anisimov, and D. Vollhardt, *Phys. Rev. B* **73**, 155112 (2006).
- [61] M. Casula, A. Rubtsov, and S. Biermann, *Phys. Rev. B* **85**, 035115 (2012).
- [62] C. Taranto, M. Kaltak, N. Parragh, G. Sangiovanni, G. Kresse, A. Toschi, and K. Held, *Phys. Rev. B* **88**, 165119 (2013).
- [63] J. M. Tomczak, M. Casula, T. Miyake, and S. Biermann, *Phys. Rev. B* **90**, 165138 (2014).
- [64] L. Boehnke, F. Nilsson, F. Aryasetiawan, and P. Werner, *Phys. Rev. B* **94**, 201106(R) (2016).
- [65] S. K. Panda, B. Pal, S. Mandal, M. Gorgoi, S. Das, I. Sarkar, W. Drube, W. Sun, I. Di Marco, A. Lindblad, P. Thunström, A. Delin, O. Karis, Y. O. Kvashnin, M. van Schilfhaarde, O. Eriksson, and D. D. Sarma, *Phys. Rev. B* **93**, 235138 (2016).
- [66] S. Backes, T. C. Rödel, F. Fortuna, E. Frantzeskakis, P. Le Fèvre, F. Bertran, M. Kobayashi, R. Yukawa, T. Mitsuhashi, M. Kitamura, K. Horiba, H. Kumigashira, R. Saint-Martin, A. Fouchet, B. Berini, Y. Dumont, A. J. Kim, F. Lechermann, H. O. Jeschke, M. J. Rozenberg *et al.*, *Phys. Rev. B* **94**, 241110(R) (2016).
- [67] F. Aryasetiawan, K. Karlsson, O. Jepsen, and U. Schönberger, *Phys. Rev. B* **74**, 125106 (2006).
- [68] K. Morikawa, T. Mizokawa, K. Kobayashi, A. Fujimori, H. Eisaki, S. Uchida, F. Iga, and Y. Nishihara, *Phys. Rev. B* **52**, 13711 (1995).
- [69] K. Yoshimatsu, T. Okabe, H. Kumigashira, S. Okamoto, S. Aizaki, A. Fujimori, and M. Oshima, *Phys. Rev. Lett.* **104**, 147601 (2010).
- [70] T. Yoshida, K. Tanaka, H. Yagi, A. Ino, H. Eisaki, A. Fujimori, and Z.-X. Shen, *Phys. Rev. Lett.* **95**, 146404 (2005).
- [71] J. Kim, J. Chung, and S.-J. Oh, *Phys. Rev. B* **71**, 121406(R) (2005).
- [72] D. Toyota, I. Ohkubo, H. Kumigashira, M. Oshima, T. Ohnishi, M. Lippmaa, M. Takizawa, A. Fujimori, K. Ono, M. Kawasaki, and H. Koinuma, *Appl. Phys. Lett.* **87**, 162508 (2005).
- [73] A. Galler, P. Thunström, P. Gunacker, J. M. Tomczak, and K. Held, *Phys. Rev. B* **95**, 115107 (2017); A. Galler, P. Thunström, J. Kaufmann, M. Pickem, J. M. Tomczak, and K. Held, *Comp. Phys. Commun.* **245**, 106847 (2019); A. Galler, J. Kaufmann, P. Gunacker, M. Pickem, P. Thunström, J. M. Tomczak, and K. Held, *J. Phys. Soc. Jpn.* **87**, 041004 (2018).
- [74] A. Toschi, A. A. Katanin, and K. Held, *Phys. Rev. B* **75**, 045118 (2007).
- [75] G. Rohringer, H. Hafermann, A. Toschi, A. A. Katanin, A. E. Antipov, M. I. Katsnelson, A. I. Lichtenstein, A. N. Rubtsov, and K. Held, *Rev. Mod. Phys.* **90**, 025003 (2018).